Defect structure of doped CaF_2 at high temperatures

C. R. A. Catlow*
Department of Chemistry, University of Keele, Keele, Staffordshire ST5 5BG, United Kingdom

A. V. Chadwick
Department of Chemistry, University of Kent at Canterbury, Canterbury, Kent CT2 7NH, United Kingdom

J. Corish
Department of Chemistry, Trinity College, Dublin 2, Ireland

L. M. Moroney
Brookhaven National Laboratory, Upton, New York 11973-5000

A. N. O'Reilly
Department of Chemistry, Trinity College, Dublin 2, Ireland
(Received 15 September 1987)

Extended x-ray-absorption fine structure (EXAFS) measurements and computer modeling techniques have been used to study defective clustering in 10 mol % CaF_2:Er^{3+}. The EXAFS spectra were recorded in the temperature range 298–1070 K and show that there is no major change, as the temperature is increased, in the structure of the hexameric $6|0|8|6_1$ cluster [P. J. Bendall *et al.*, J. Solid State Chem **51**, 159 (1984)] which has been previously identified in CaF_2:Er^{3+}. The computer simulation calculations have been extended to evaluate the dipole moments of the clusters suggested previously and to study a number of other clusters which have been suggested as being responsible for the observed dielectric relaxation and electronic spectra. The new data presented here are discussed in conjunction with the other available experimental evidence and a mechanism is suggested for the generation of the additional mobile species necessary to explain the high-temperature conductance.

I. INTRODUCTION

Dopant-interstitial clustering in anion-excess alkaline-earth fluorides has been studied by a wide range of techniques in recent years. The complexity of the cluster structures has been revealed by diffraction,[1,2] spin resonance,[3,4] spectroscopic,[5–7] extended x-ray-absorption fine structure EXAFS,[8,9] and computer modeling techniques.[10,11] The simple tetragonal and trigonal dopant-interstitial monomers which dominate at very low concentrations (0.1 mol % dopant) are considered to be replaced at higher concentrations by dopant dimers and trimers, Figs. 1 and 2, and by the hexameric species illustrated in Fig. 3. Ordering of the latter type of cluster leads to superstructure which have been detected in the diffraction studies of Greis and co-workers.[12,13]

Despite the extensive range of studies there are still several problems with our understanding of these systems. Firstly, although the formation of the clusters related to the hexameric structure in Fig. 3 is well established, the precise structure of such clusters is still uncertain. Secondly, the behavior of the materials at higher temperatures is not understood. In their conductivity studies Archer *et al.*[14] find a rapid increase in the ionic conductivity at 870 K (cf. Fig. 4), and evidence for significant displacements of clustered interstitials at these temperatures has been provided by neutron studies.[15]

Much of the information on impurity-defect aggregates in the alkaline-earth fluorides has been obtained from spectroscopic and dielectric relaxation techniques,[16–18] the latter technique being sensitive to aggregates with a dipole moment which can reorientate through migration of the anions. The most thoroughly investigated system is CaF_2:Er^{3+} which exhibits five dielectric relaxations, R-I to R-V (designated "RI" to "RV" by Fontanella and Andeen[17]), and at least 16 erbium sites have been identified in the electronic spectra.[19] The RI relaxation

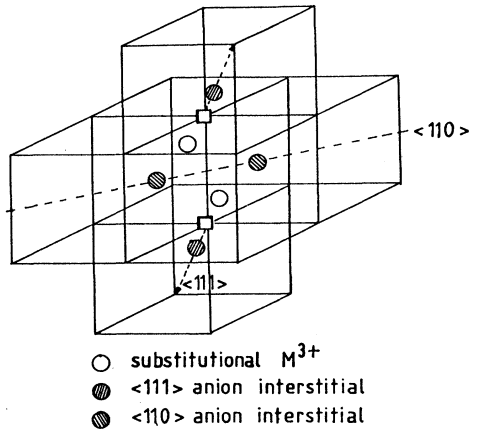

FIG. 1. Schematic representation of the $2|0|2|_1$ dimer.

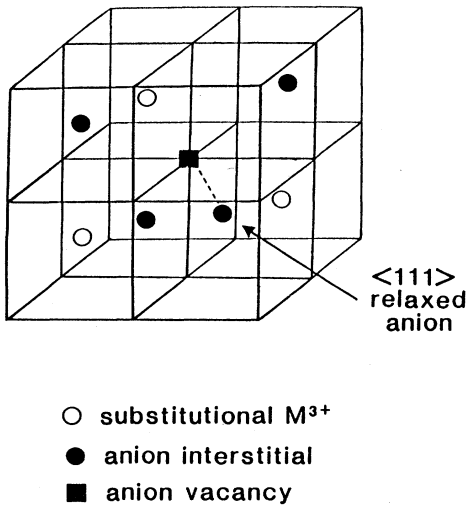

FIG. 2. Schematic representation of the $3|0|1|3_1$ trimer.

has been identified as the simple tetragonal dopant–near-neighbor monomer. In crystals containing 10% erbium there is only one relaxation, R-III (Ref. 16) and only one component in the electronic spectrum, the $D(2a,b)$ pair in the nomenclature of Moore and Wright.[7] Defects responsible for the $D(2)$ spectra contain at least three rare-earth ions[20] and therefore the R-III relaxation is due to a large cluster which possesses a dipole moment and two types of erbium site. The structure of the cluster responsible for the R-III relaxation and the origin of the R-II relaxation have been discussed by Welsh.[21]

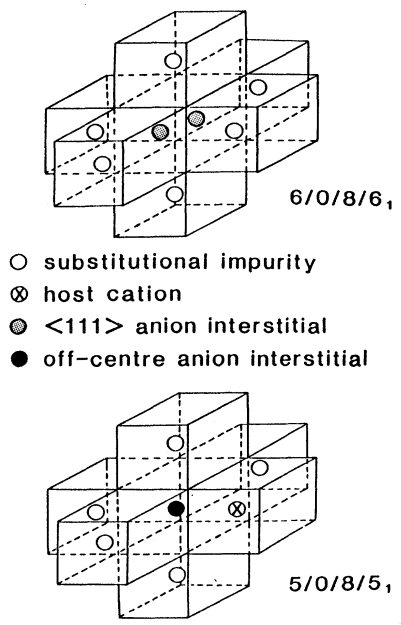

FIG. 3. Schematic representations of the hexamer $6|0|8|6_1$ and pentamer $5|0|8|5_1$ clusters: only the cube-center anion interstitials are shown.

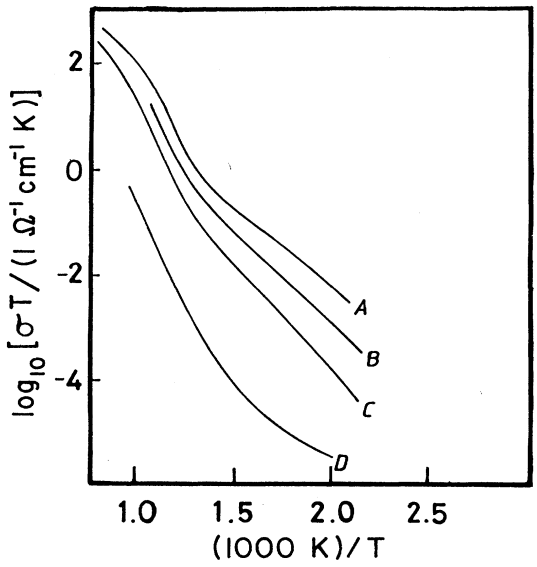

FIG. 4. Ionic conductivity of $CaF_2:Er^{3+}$ measured by Archer *et al.* (Ref. 14).

The aim of the present study is to use EXAFS measurements and computer modeling studies to further elucidate the defect cluster structure of 10 mol% $CaF_2:Er^{3+}$. Firstly we will examine, using EXAFS, the temperature dependence of the cluster structure. Secondly, the computer modeling techniques, including the calculation of dipole moments, will be extended to model clusters that can provide assignments for the observed relaxation modes. The results of these studies are also used, in conjunction with our earlier neutron work, to suggest mechanisms for the generation of the additional mobile species necessary to account for the high-temperature conductivity.

II. TECHNIQUES AND RESULTS

A. Computer modeling

The methods used to calculate defect energies are exactly as in our previous studies of these systems.[10,11] We employed the generalized Mott-Littleton procedure available in the HADES III code using the potentials derived by Catlow *et al.*[22] The number of ions in region I was approximately 180, which is sufficiently large for the present study. The HADES program has recently been extended[23] to enable it to calculate the dipole moment of the defect species under consideration. The method sums all the dipoles which result both from the defect configuration and the lattice relaxation and includes the effects of ionic polarization.

To rationalize the high-temperature properties and the assignments made by Welsh[21] it is necessary to consider dopant pentamers and tetramers (both with varying numbers of interstitials) in addition to the hexamer shown in Fig. 3; we must also investigate the monomer with C_{3v} symmetry, Fig. 5, that was considered by Welsh to be re-

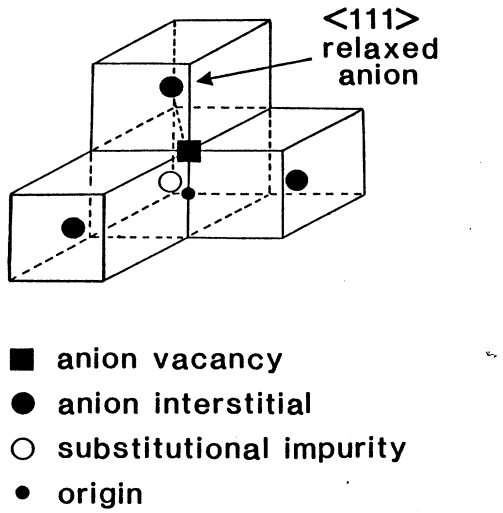

FIG. 5. Schematic representation of the monomer $1|0|1|2_1$ showing the ⟨111⟩ relaxed anion. The coordinate of this anion relative to the lattice site from which it has relaxed are −0.349, −0.349, and 0.858.

sponsible for the observed R-II relaxation mode measured in dielectric relaxation studies.[16–18] In the nomenclature described by Bendall *et al.*[11] (cf. Appendix) the specific clusters for which results are presented here are the following.

(i) The $5|0|8|5_1$ and the $5|0|8|4_1$ pentamers and the $4|0|8|5_1$ tetramer.

(ii) The $1|0|1|2_1$ monomer which is the trigonal cluster shown in Fig. 5.

The calculated energies and, dipole moments of the relevant clusters, are reported in Table I, which gives the total energies for these clusters as well as their association energies in eV per trivalent ion. In addition, we report results for the $6|0|8|6_1$, $6|0|8|5_1$, and $1|0|0|2_1$ clusters, which we have considered previously. Comparison of these values shows that the trigonal $1|0|1|2_1$ monomer is lower in energy than the closely related $1|0|0|2_1$, and that the $5|0|8|5_1$ has a slightly larger binding energy than the $6|0|8|6_1$.

TABLE I. Defect energies in eV, association energies in eV/M^{3+}, and dipole moments in e Å, for the specified clusters in CaF_2:Er^{3+}.

Cluster	Defect energy	Association energy	Calculated dipole moment
$1\|0\|1\|2_1$	−25.556	−1.165	
$1\|0\|1\|2_1$	−25.645	−1.253	0.38
$2\|0\|0\|1_1$	−43.262	−0.379	
$3\|0\|4\|5_1$	−75.363	−1.427	
$4\|0\|8\|5_1$	−97.325	−1.509	
$5\|0\|8\|4_1$	−113.398	−0.799	
$5\|0\|8\|5_1$	−118.295	−1.360	1.48
$6\|0\|8\|5_1$	−138.667	−1.112	
$6\|0\|8\|6_1$ ⟨111⟩	−141.441	−1.275	0.00

B. EXAFS measurements

The EXAFS technique is now a well-established method for obtaining information on the local environment of particular atomic species in disordered materials. We have recently reported a detailed application of EXAFS to the study of defect clustering in alkaline-earth fluorides at low temperatures.[8,9] In the EXAFS experiment we measure the fine structure adjacent to x-ray-absorption edges arising from excitations from core levels. This fine structure is due to the interference of the backscattered components of the photoelectron with the propagating photoelectron wave. It has been shown[24] that the fine structure χ can be expressed by the following equation:

$$\chi=\sum_j \left[\frac{N_j}{kR_j^2}\right] \exp(-2\sigma_j^2 k^2)|f_j(\pi)| \exp(-2R_j/\lambda) \times \sin(2kR_j+2\delta+\psi_j) \,. \quad (1)$$

This standard equation is essentially the product of an amplitude function and a frequency function. The amplitude of the oscillations depends directly on the number of atoms in the jth shell and inversely on R_j, where R_j is the distance of those neighbors from the absorbing atom. The term $f_j(\pi)$ describes the backscattering power of the neighboring atoms, is a k-dependent function (photoelectron wave number), and varies with the number of electrons in the backscattering atom. The term σ^2 which is contained in the first exponential factor takes account of the loss in amplitude caused by thermally induced and static displacements within the jth shell. In fact, σ^2 is the mean-square fluctuation in the interatomic distance between the atom at the origin and the jth atom. The fluctuations include a dynamical term due to thermal motion of the atoms and a static term due to structural disorder. The temperature dependence of σ^2 is pertinent to the present study and must be considered. When only dynamical fluctuations due to thermal disorder are of importance it is expected that σ^2 should show a linear dependence on temperature.[25] However, if the static term due to structural disorder is significant, then an anomalous feature should be observed in the temperature dependence of σ^2.

The second exponential term accounts for the decay of the photoelectron as it propagates through the lattice. $\lambda(k)$ represents the mean free path of the electrons which will increase with increasing photoelectron wave vector k.

The frequency function which varies with k contains the anticipated sine term to generate the oscillatory nature of χ, and the frequency of the oscillations decreases as the radial distance R_j, between the emitter and backscatter, decreases. The phase alteration which the photoelectron wave experiences when it interacts with the electronic potential of the excited and backscattering atoms is included in the factors 2δ and ψ_j, respectively. The phase shifts are functions of k and hence of the kinetic energy of the electron ejected in the absorption process.

In our previous EXAFS study[8] of 10 mol% Er^{3+}-doped CaF_2 we showed that the data were con-

sistent with the $6|0|8|6_1$ cluster, unlike the case for La^{3+}-doped CaF_2 where the spectra were interpreted more satisfactorily as arising from $2|0|2|3_1$ clusters. In the present study we extend our previous work on CaF_2:Er^{3+} both by collecting new data at high temperatures and by examining the consistency of these and the previous room-temperature data with other clusters indicated by different experimental techniques.

C. Experimental method and data analysis

The sample used was a portion of a single crystal of CaF_2:Er^{3+} which was grown by a modified Stockbarger technique: the dopant concentration was 10 mol % erbium. The required sample thickness, which would allow a photo transmission rate of at least 30%, was achieved by diluting the sample with boron nitride. The sample and dilutant were ground to a fine homogeneous powder and then pressed under 8 tons to a disk of radius 0.5 cm. The disk was then mounted in a sample holder which was surrounded by a heating element, and this unit was placed in an EXAFS furnace-cryostat with beryllium windows. The furnace was then evacuated to 10^{-4} torr. The EXAFS spectra were measured over a range of temperatures from 298 to 1070 K, using the synchrotron radiation source at Daresbury Laboratory. During these experiments, the synchrotron operated at an energy of 2.0 GeV. Data were obtained at erbium L_{III} edge and were measured in the transmission mode at station 7.1.

The data were normalized and the background subtracted and fitted using programs from the Synchrotron Radiation Source (SRS) Library at Daresbury. Initially the strategy adopted was based on a comparative qualitative analysis of the data without recourse to theoretical models. Data analysis proper was facilitated by an interactive program package EXCURVE which uses the curved-wave theory in the EXAFS phenomenon to generate theoretical spectra from model structures. This program enabled us to effect the Fourier transformation of spectra from frequency to distance space. The use of Fourier filtering separated the complex EXAFS spectrum into peaks representing each component frequency or backscattering from an individual shell. The analysis also made use of the facility which allows an iterative least-squares fitting procedure to adjust parameters within certain defined limits. This ensured that the sum of the squares of the difference between the experimental and theoretical plots was minimized.

D. Experimental results

A total of eight spectra were recorded over the temperature range 298–1070 K. The presentation of the results will be confined, however, to the spectra recorded at 298, 738, and 1070 K, since they provide the necessary features.

Initially, a qualitative assessment of the results can be made by examination of the raw data. The raw EXAFS in k space and corresponding Fourier-transformed data in R space of the chosen spectra are shown in Figs. 6–8. The damping of the EXAFS at high energy necessitated the k^3 weighting over the entire range in order to enhance the high-energy region of the spectra. A comparative examination of these spectra reveals the presence of four well-defined peaks at the low-energy side of the spectra. Above this, the data become less structured despite the k^3 weighting. As expected, there is also a decrease in the signal-to-noise ratio as the temperature is increased. Apart from a smearing out of structure at high temperatures, the basic pattern remains the same in all the spectra. On the high-energy side of the second peak, however, there is a small sharp peak which progressively diminishes over the temperature range, appearing only as a slight shoulder at higher temperatures. Similarly, there is another intervening feature between the third and fourth peak which behaves in a similar fashion. While the amplitude of the data is seen to decrease gradually with temperature, the frequency of the oscillations remains the same.

Examination of the corresponding Fourier-transformed data for each spectrum (which were obtained without calculation of phase shifts) is a useful but again qualitative intermediate step. The omission of these appropriate

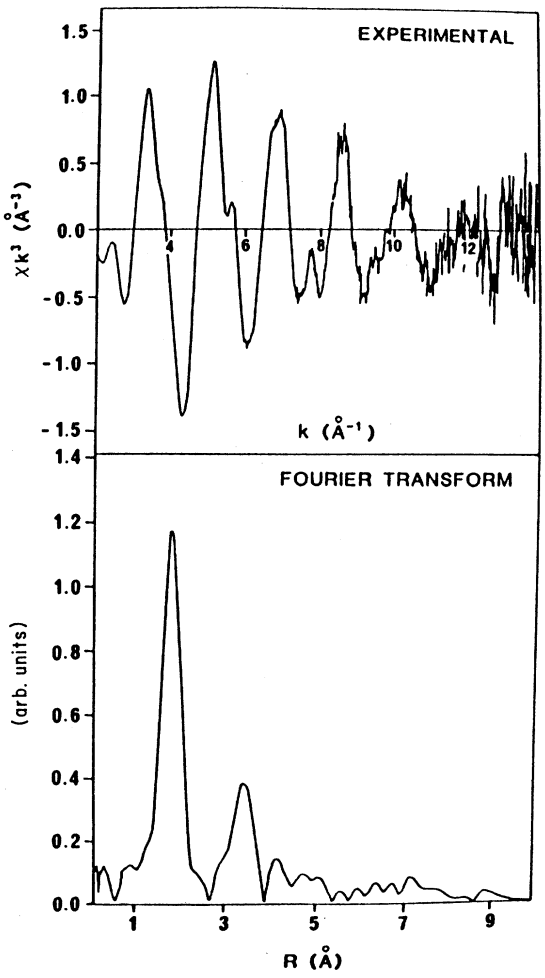

FIG. 6. Raw EXAFS data for CaF_2:Er^{3+} at 298 K: the Fourier transform of these data into R space is also shown.

phase shifts causes the peaks, representing the shell distances, to be displaced from their correct positions. A more illuminating handling of the data requires the application of the technique of Fourier filtering. This involves the isolation of a single peak in the Fourier transformation, and in this analysis, only the first shell was considered. Although contributions from more distant shells were found to be significant in our previous study,[9] an analysis in terms of the first shell alone is sufficient to determine whether there are major changes in cluster structure. The single peak in the Fourier transform was then backtransformed into k space so that the component sinusoidal wave of the EXAFS, corresponding to backscattering from the first shell of atoms, could be displayed. The Fourier-filtered data of the previously discussed EXAFS spectra are presented in Figs. 9–11. Again the Fourier transformations were calculated in the absence of the phase shifts, and so the absolute positions of the maxima do not have any significance. The primary aim of this step in the analysis is to reveal any change in frequency which may occur in k space. The effect of temperature on CaF_2 causes an expansion of the lattice from 2.722 Å at 0 K to 2.798 Å at 1070 K. Thus in the absence of any other structural alteration, an increase in radial distance should be observed with a consequent increase in the frequency of the spectra recorded at high temperatures. When the Fourier filtered data of the spectra recorded at 298 and 1070 K are superimposed, any change in frequency can clearly be observed. In fact, the frequency of the high-temperature spectra decreases slightly. Inclusion of the intervening spectra reveals that this is a gradual process. In addition, it was noted that the decrease in amplitude of the peaks at high k is faster than at low k.

The next step in the analysis of the data produces a quantitative assessment of the situation. This time the Fourier transformation of the data was calculated using the appropriate phase shifts obtained in our previous study[8] using a semiempirical procedure. In addition, using the $6|0|8|6_1$ ⟨111⟩ cluster as a starting model, a

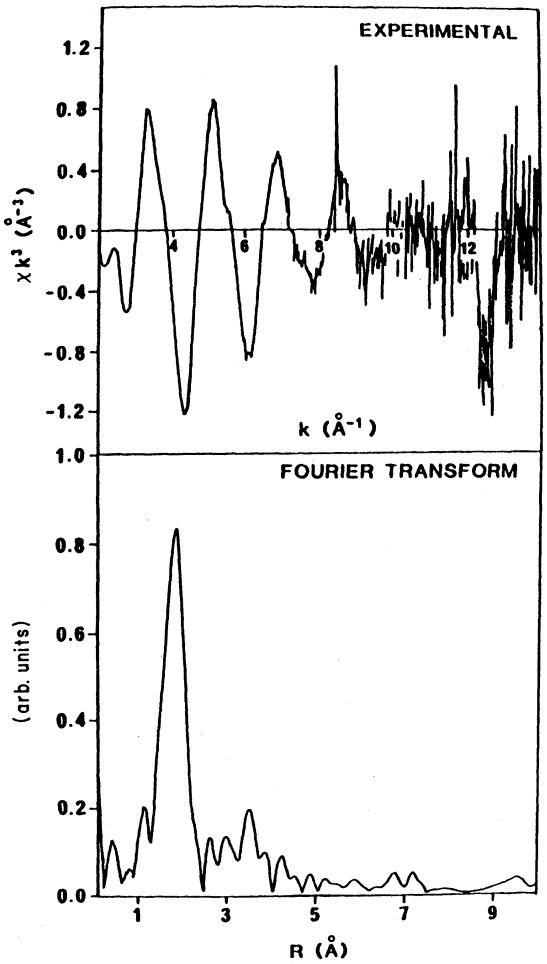

FIG. 7. Raw EXAFS data for CaF_2:Er^{3+} at 738 K: the Fourier transform of these data into R space is also shown.

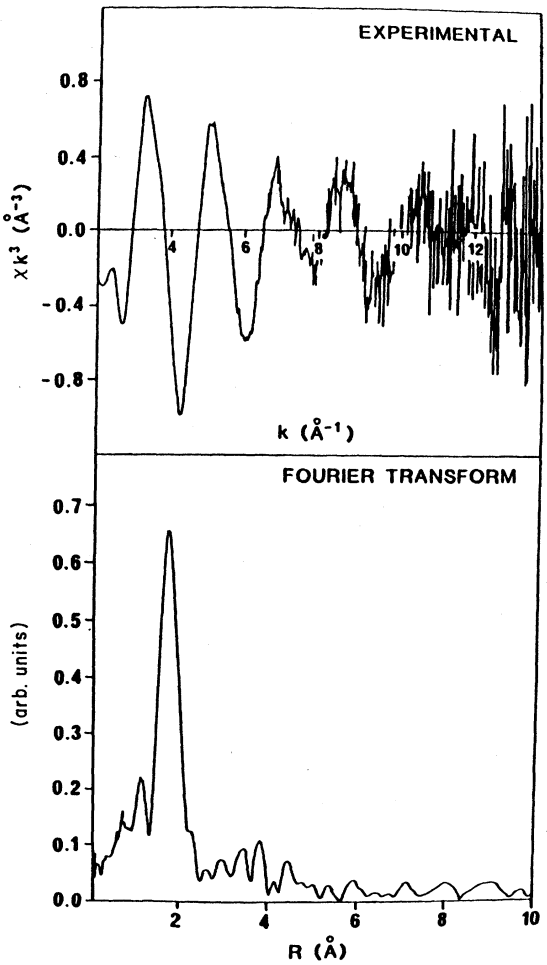

FIG. 8. Raw EXAFS data for CaF_2:Er^{3+} at 1070 K: the Fourier transform of these data into R space is also shown.

least-squares-fitting procedure adjusted the input values of N_j, R_j, and A_j, which are the number of atoms in the shell j, the radial distance of shell j and the Debye-Waller factor, respectively, in order to minimize the difference between the experimental and theoretical spectra. The resulting values of A_1 and R_1 from all the recorded spectra are shown in Table II. The plots of the theoretical versus experimental spectra recorded at 298 and 1070 K are given in Figs. 12 and 13, respectively. Examination of the results given in Table II shows that the radial distance remains unchanged over the entire temperature range, giving a constant value of 2.33 Å. In contrast, the Debye-Waller factor increases with temperature linearly, as shown in Fig. 14.

Closer examination of the coplot of the theoretical and experimental spectra reveals that, while at low temperature the agreement between theory and experiment is excellent, the peaks at high k in the spectra recorded at elevated temperatures are slightly offset from the corresponding theoretical peaks. In addition, the peak in R space at high temperature is shifted to slightly lower R. Since this peak shifts inwards and a shoulder is also seen to develop on its left side, the possibility of an asymmetrical distribution function must be considered. At this stage it is worth referring to a similar analysis by Boyce and Hayes[26] on the superionic phase of AgI at 471 K. They found that in order to obtain adequate fitting of the data at high temperatures it was necessary to allow for an asymmetrical distribution about the central ion by going from a single-Gaussian to a 3:1 two-Gaussian peak model. This means that while a Gaussian distribution function is adequate at low temperatures to describe the distribution of the atoms in the first shell, it breaks down at higher temperatures due to thermal disorder.

With this in mind, the final refinement in the data reduction was applied. This involved the examination of the ability of a superposition of Gaussian distribution functions to produce the observed behavior of the EXAFS, especially at high temperatures. For the low-temperature data a single-Gaussian function was com-

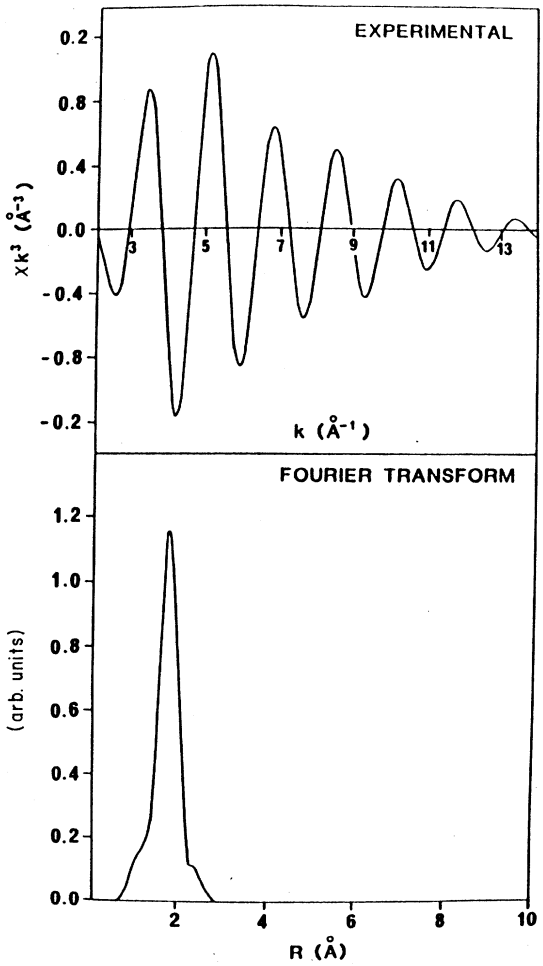

FIG. 9. Fourier-filtered first shell of the backscatterers and the backtransform of these data into k space to give the component sinusoidal wave of the EXAFS data recorded at 298 K.

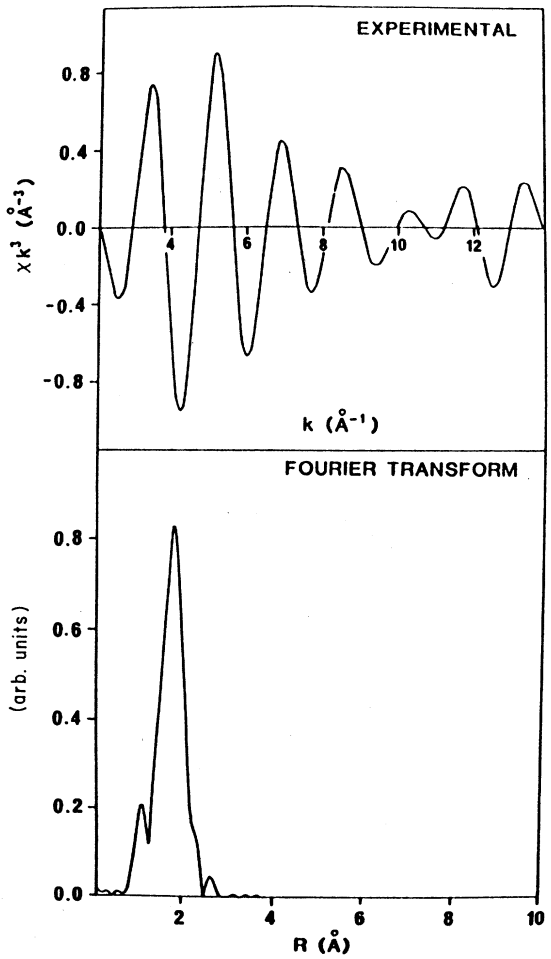

FIG. 10. Fourier-filled first shell of backscatterers and the backtransform of these data into k space to give the component sinusoidal wave of the EXAFS data recorded at 738 K.

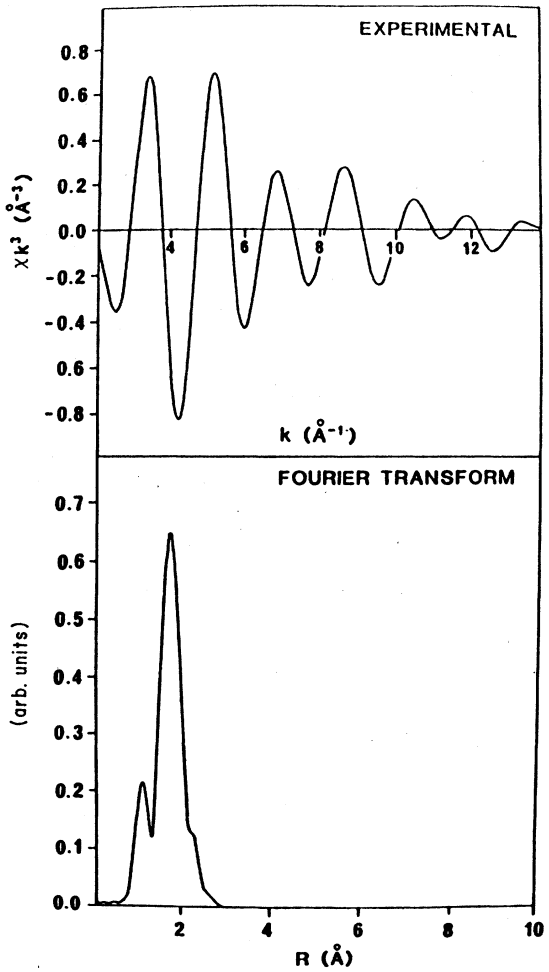

FIG. 11. Fourier-filtered first shell of backscatterers and the backtransform of these data into k space to give the component sinusoidal wave of the EXAFS data recorded at 1070 K.

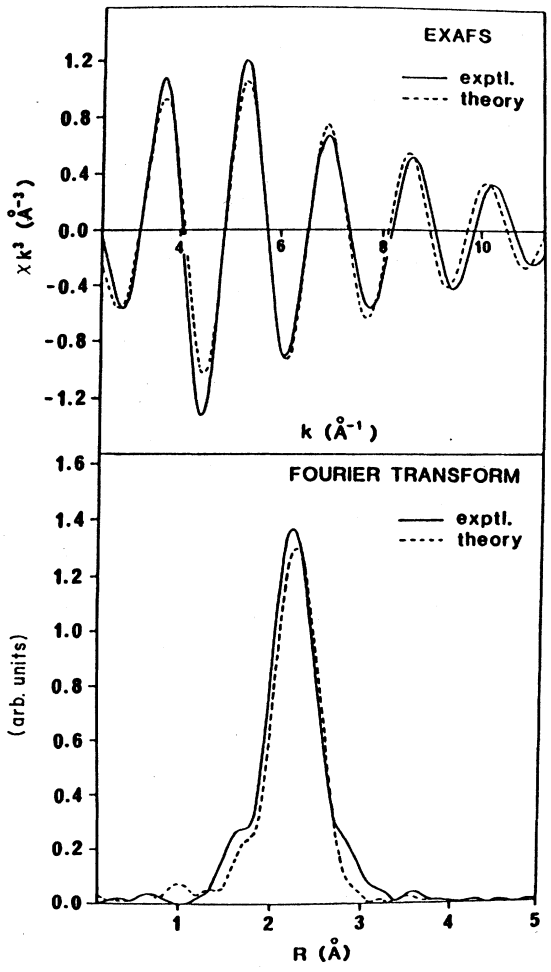

FIG. 12. Fourier transform, calculated using the appropriate phase shifts, of the first shell of backscatterers and the corresponding backtransform into k space to give the component sinusoidal wave of the EXAFS data recorded at 298 K. The $6|0|8|6_1\ \langle 111\rangle$ cluster was used as a starting model and least-squares fitting was used to adjust the input values of N_1, R_1, and A_1 to minimize the difference between the experimental and theoretical spectra.

pared with a split-shell Gaussian function of equal amplitude. Thus, in the first case, the coordination around the central erbium was assumed to be nine fluoride ions with a mean single distance, and in the second instance it was assumed that the shell was split into two parts each, with 4.5 fluoride ions surrounding the central erbium. The fitted values are given in Table III, while the plots of the theory versus the experiment are given in Fig. 15. In fact, the split-shell model gives only a slight improvement on the single-shell model, particularly at high k, for the low-temperature data.

TABLE II. Values for the radial distance R_1 (Å) and Debye-Waller factor A_1 (Å^2), for the first shell of backscatterers in the $6|0|8|6_1\ \langle 111\rangle$ cluster, as a function of temperature.

Temperature (K)	R_1	A_1
298.0	2.33	0.018
493.0	2.33	0.022
723.0	2.32	0.026
897.0	2.31	0.029
973.0	2.33	0.031
1066.0	2.33	0.032

Similar consideration of the spectra recorded at 1070 K, however, gives a different result. Table III presents the values for R_1 and A_1, while Fig. 15 gives the coplot of the theory versus experiment for the one- and two-shell models, respectively. The frequency of the experimental EXAFS at high k is matched more closely in the split-shell model, as is the radial distribution function. In addition, the amplitude difference between the theoretical and experimental profiles has been reduced.

III. DISCUSSION

Let us first consider the implications of the EXAFS data. These suggest that there is no major change in clus-

ter structure at higher temperatures. We note that the frequency of oscillations alters only slightly as the temperature increases, indicating that the changes in the EXAFS can be attributed largely to an increase in the amplitudes of thermal motion. At higher temperatures it does seem necessary to use a split-shell model to fit the data, assuming formation of the $6|0|8|6_1$ cluster. But, as pointed out by Hayes and Boyce,[27] non-Gaussian peak shapes may be expected with large amplitude vibrations at high temperatures in superionic conductors.

It appears therefore that the $6|0|8|6_1$ cluster can account for the EXAFS data between 298 and 1070 K. Three questions follow: the first asks whether related clusters could equally well be used to fit the data; the second concerns the ability of this cluster to account for other experimental observations; and the third relates to the observed high-temperature conductivity, which clearly indicates the injection of additional carriers or the onset of a new conduction mechanism.

As regards the first point, we have calculated EXAFS spectra for the $6|0|8|6_1$ and $5|0|8|5_1$ clusters on CaF_2:Er^{3+}. The differences between these two spectra are very small indeed and certainly could not be detected experimentally. The $5|0|8|5_1$ is clearly therefore also a plausible cluster model for CaF_2:Er^{3+}. Moreover, we note that its calculated binding energy per impurity ion (Table I) slightly exceeds that of the corresponding $6|0|8|6_1$ cluster. Our dipole-moment calculations show that the $5|0|8|5_1$ cluster, in contrast to the $6|0|8|6_1$, has a dipole moment, so that, provided it can reorientate, it can also account for the B-III relaxation peak, as suggested by Welsh.[2] We should note, however, that the reorientation of the cluster requires there to be equivalent dipolar interstitial configurations. Our calculations have not found such configurations but show that the central interstitial (cf. Fig. 3) is located on the C_4 axis of the cluster. A further point which supports the $5|0|8|5_1$ as the probable source of the R-III relaxation peak is the fact that the cluster contains two types of rare-earth site, which is consistent with the observation of the $D(2a)$ and $D(2b)$ electronic transitions.[7] Welsh has already argued that these $D(2)$ transitions detected in the laser spectroscopy studies arise from the defect cluster, as does the R-III dielectric relaxation mode.

We recall that Welsh[21] has also assigned the observed R-II dielectric relaxation mode to a cluster with trigonal symmetry. Our calculations would strongly suggest that

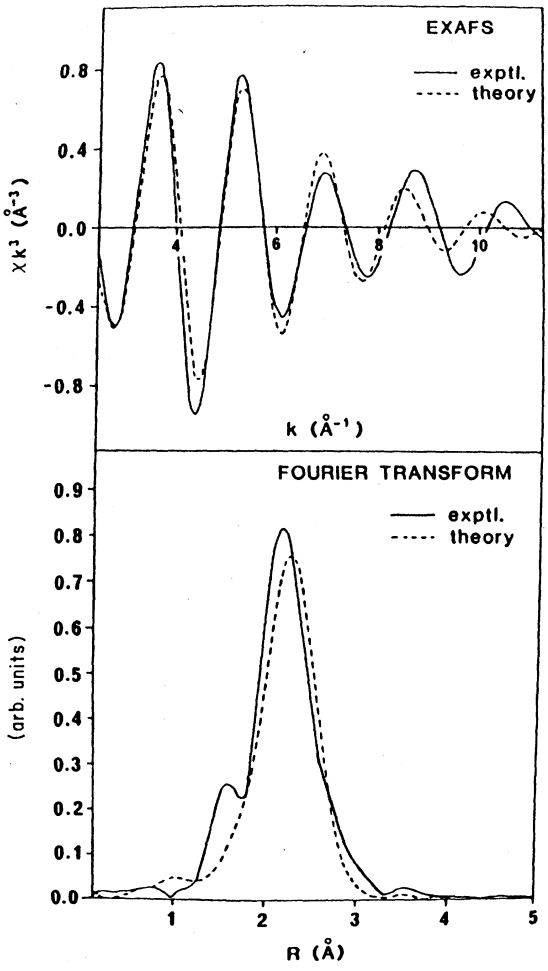

FIG. 13. Fourier transform, calculated using the appropriate phase shifts, of the first shell of backscatterers and the corresponding backtransform into k space to give the component sinusoidal wave of the EXAFS data recorded at 1070 K. The $6|0|8|6_1$ ⟨111⟩ cluster was used to adjust the input values of N_1, R_1, and A_1 to minimize the difference between the experimental and theoretical spectra.

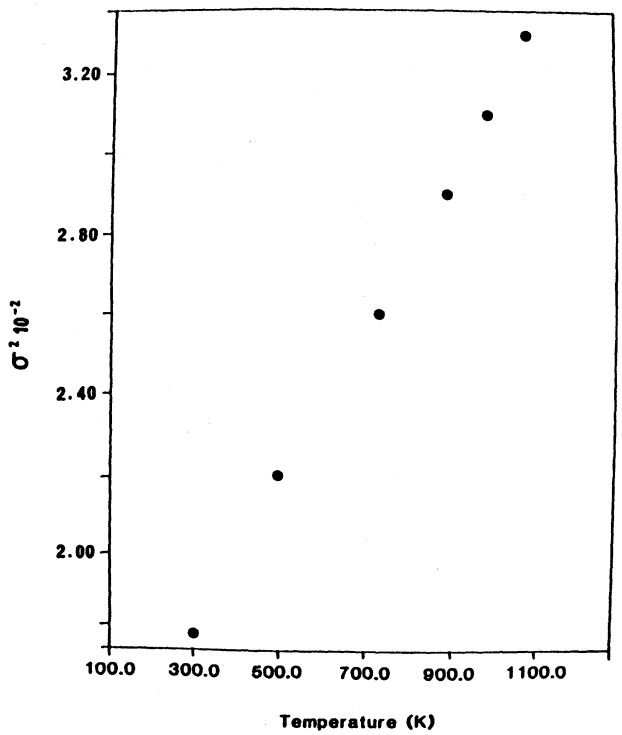

FIG. 14. Temperature dependence of the Debye-Waller factor A_1 (Å^2) for the first shell of backscatterers in the $6|0|8|6_1$ cluster in CaF_2:Er^{3+}.

TABLE III. A comparison of the values for the radial distances R_1 and R_2 (Å) and Debye-Waller factors A_1 and A_2 (Å^2) obtained using a single or split-shell Gaussian function to describe the distribution of the first shell of backscatterers in the $6|0|8|6_1$ ⟨111⟩ cluster at 298 and 1070 K. N_1 and N_2 refer to the number of fluoride ions assigned to the first and second components of the split shell, respectively.

Temperature (K)	N_1	N_2	R_1	R_2	A_1	A_2
298.0	9		2.33		0.018	
298.0	4.5	4.5	2.28	2.40	0.008	0.013
1070.0	9		2.33		0.038	
1070.0	4.5	4.5	2.27	2.44	0.013	0.020

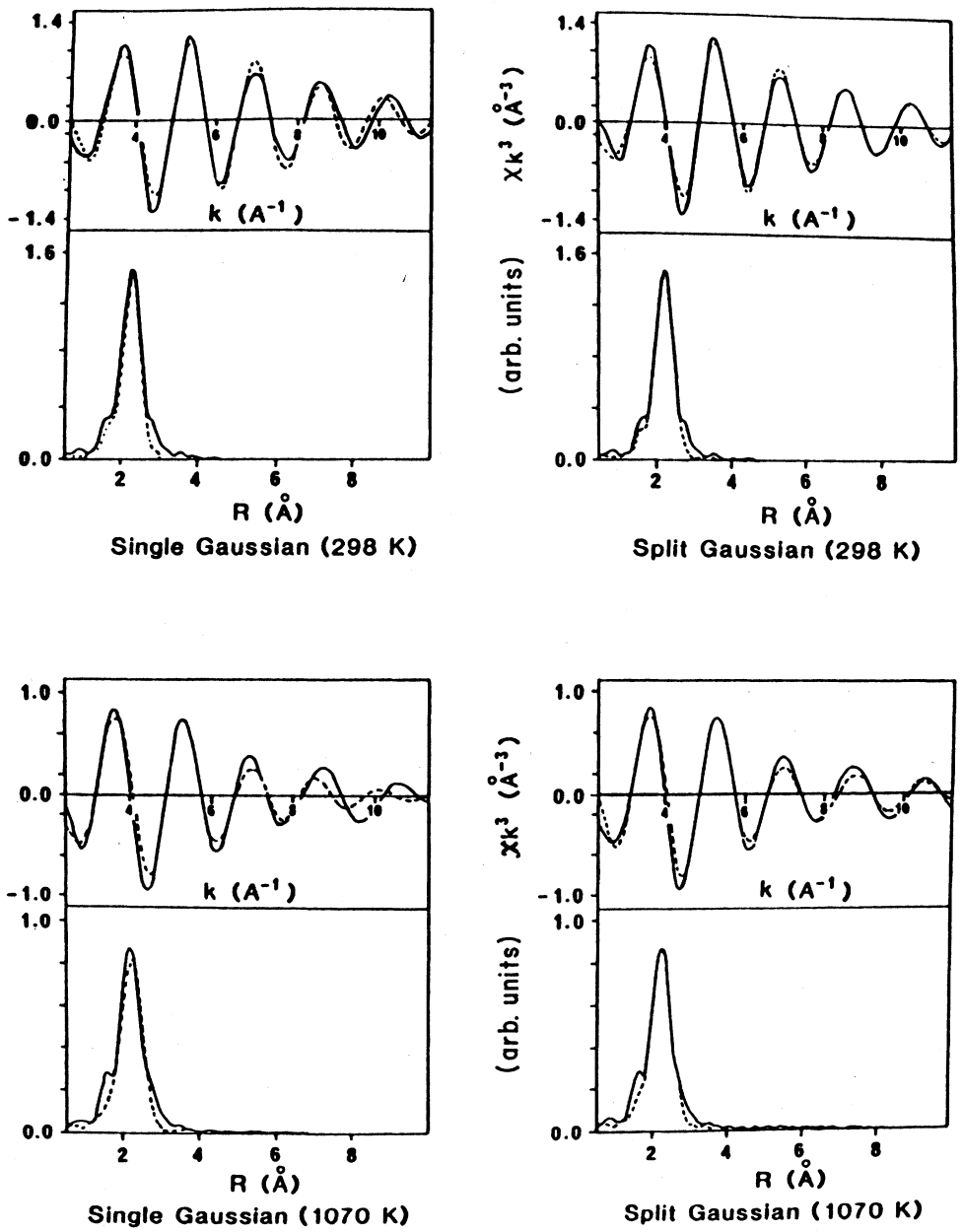

FIG. 15. Comparison of the abilities of a single-shell and two split-shell Gaussian functions to reproduce the experimental EXAFS spectra of the first shell of backscatterers in the $6|0|8|6_1$ cluster in CaF_2:Er^{3+}. The experimental lines are shown as —— and the theoretical lines as — — —.

the $1|0|1|2_1$ cluster shown in Fig. 5 is responsible for this relaxation mode, and again we note from Table I that this species has a dipole. From the structure shown in Fig. 5 it would be expected that reorientation can readily occur.

We now return to the problem of the high-temperature conductivity exhibited by trivalently doped CaF_2. The EXAFS results indicate that the onset of the rapid increase in conductivity cannot be accounted for by major disruption of the clusters to yield mobile species. One possible mechanism for the injection of mobile interstitials without cluster dissociation would involve the loss of interstitials from the central cube (see Fig. 3) of the hexameric or pentameric clusters. The processes could be represented by the following reactions:

$$6|0|8|6_1 \rightarrow 6|0|8|5_1 + 0|0|0|1 \ , \tag{2a}$$

$$5|0|8|5_1 \rightarrow 5|0|8|4_1 + 0|0|0|1 \ . \tag{2b}$$

From the calculated energies in Table I we obtain energies of 0.68 and 2.8 eV for reactions (2a) and (2b), respectively. The value obtained for reaction (2a) is sufficiently small to make this process a plausible model for the injection of mobile defects at high temperatures. In contrast, the value for reaction (2b) is prohibitively large.

The removal of an interstitial from the central cube of the $6|0|8|6_1$ cluster might be expected to give rise to an inward displacement of the 12 surrounding $\langle 110 \rangle$ interstitials towards the central cube edge. Our calculations find an average inward displacement of ~ 0.055 Å for these species, but it should be noted that in the $6|0|8|6_1$ these interstitials are not all equivalent. The earlier neutron diffraction data[15] showed that the major change that was observed on heating CaF_2:Er^{3+} from 80 to 1125 K also involved the displacement of the $\langle 110 \rangle$ interstitials by ~ 0.083 Å, again towards the central cube edge.

Of course, from our previous arguments it is clear that the $6|0|8|6_1$ cluster cannot be present alone. It is indeed highly plausible that several different cluster models will coexist. Furthermore, the multiple lines that appear in the optical spectra, and which are due to crystallographically inequivalent ions, are likely to arise from the various stages in the formation of the complete hexamer.

IV. CONCLUSIONS

The three most important features to emerge from this study are the following: first, the results of the EXAFS study show that the large dopant aggregates previously identified at room temperature persist to high temperatures. Secondly, the extension of the computer modeling to new defect clusters has shown that the trigonal $1|0|1|2_1$ cluster and the $5|0|8|5_1$ pentameric cluster proposed by Welsh as responsible for the R-II and R-III dielectric relaxation modes, respectively, do have dipole moments and are stable, although we have not found a relaxation mode for the $5|0|8|5_1$ cluster. Thirdly, we propose that the onset of enhanced conductivity at ~ 870 K can be attributed to the release of interstitials from clusters such as the $6|0|8|6_1$. We have shown that this cluster has an interstitial whose binding energy is sufficiently low to permit release at higher temperatures. We should stress that the defect structure of these materials is complex and that several cluster types will coexist at all but the most dilute dopant concentrations.

ACKNOWLEDGMENTS

We wish to thank Dr. G. N. Greaves for assistance with the EXAFS experiments. A.N.O'R. acknowledges partial support from the Irish Department of Education.

APPENDIX

The notation to describe the clusters in trivalently doped fluorites introduced by Bendall *et al.*[11] denotes a cluster by the symbols

$$i|v|p|q_r s_t \cdots \ ,$$

where i denotes the number of trivalent substitutional impurity ions, v the number of vacancies, p the number of relaxed lattice anions, q the number of interstitials in *nn* sites ($r=1$), and s the number of interstitials in *nnn* sites ($t=2$). It should be noted that this notation distinguishes between a vacancy and a vacant site which results from the relaxation of a lattice ion. In the case of the $6|0|8|6$ hexamer the orientation adopted by the two interstitial ions in the central cube is denoted as $\langle 111 \rangle$ following the symbols for the cluster.

*Author to whom correspondence should be addressed.

[1]O. Greis and D. J. M. Bevan, J. Solid State Chem. **24**, 113 (1978).
[2]A. K. Cheetham, B. E. F. Fender, and M. J. Cooper, J. Phys. C **4**, 3107 (1971).
[3]E. Secemski and W. Low, J. Chem. Phys. **64**, 4240 (1976).
[4]F. K. Fong, J. Chem. Phys. **64**, 4243 (1976).
[5]J. M. Baker, E. R. Davies, and J. P. Hurrell, Proc. R. Soc. London Scr. A **308**, 403 (1968).
[6]D. R. Tallant, D. S. Moore, and J. C. Wright, J. Chem. Phys. **67**, 2897 (1977).
[7]D. S. Moore and J. C. Wright, J. Chem.. Phys. **74**, 1626 (1981).
[8]C. R. A. Catlow, A. V. Chadwick, G. N. Greaves, and L. M. Moroney, Radiat. Eff. **75**, 159 (1983).
[9]C. R. A. Catlow, A. V. Chadwick, G. N. Greaves, and L. M. Moroney, Nature **312**, 601 (1984).
[10]J. Corish, C. R. A. Catlow, P. W. M. Jacobs, and S. H. Ong, Phys. Rev. B **25**, 10 (1982); **25**, 6425 (1982).

[11]P. J. Bendall, C. R. A. Catlow, J. Corish, and P. W. M. Jacobs, J. Solid State Chem. **51**, 159 (1984).
[12]O. Greis, in the Fourteenth Rare Earth Research Conference, Fargo, 1979 (unpublished).
[13]W. Gettman and O. Greis, J. Solid State Chem. **26**, 255 (1978).
[14]J. A. Archer, A. V. Chadwick, I. R. Jack, and B. Zegiri, Solid State Ionics **9&10**, 505 (1983).
[15]C. R. A. Catlow, A. V. Chadwick, and J. Corish, Radiat. Eff. **75**, 61 (1983).
[16]C. G. Andeen, J. J. Fontanella, M. C. Wintersgill, P. J. Welcher, R. J. Kemble, and G. E. Matthews, J. Phys. C **14**, 3557 (1981).
[17]J. J. Fontanella and G. G. Andeen, J. Phys. C **9**, 1055 (1976).
[18]J. J. Fontanella, D. J. Treacy, and C. G. Andeen, J. Chem. Phys. **72**, 2235 (1980).
[19]D. R. Tallant and J. C. Wright, J. Chem. Phys. **75**, 2074 (1975).
[20]M. B. Seelbinder and J. C. Wright, J. Chem. Phys. **75**, 5070 (1981).
[21]H. K. Welsh, J. Phys. C **18**, 5637 (1985).
[22]C. R. A. Catlow, M. J. Norgett, and T. A. Ross, J. Phys. C **10**, 1063 (1977).
[23]J. Corish, P. B. Fitzsimons, and P. W. M. Jacobs, Philos. Mag. A **56**, 456 (1987).
[24]P. A. Lee and J. B. Pendry, Phys. Rev. B **11**, 2795 (1975).
[25]W. Bohmer and P. Rabe, J. Phys. C **12**, 2465 (1979).
[26]J. B. Boyce and T. M. Hayes, in *Physics of Superionic Conductors,* edited by M. B. Salamon (Springer-Verlag, New York, 1979).
[27]T. M. Hayes and J. B. Boyce, Solid State Phys. **37**, 173 (1982).